

Cite this: *Mater. Horiz.*, 2019,
6, 788Received 3rd January 2019,
Accepted 14th January 2019

DOI: 10.1039/c9mh00008a

rsc.li/materials-horizons

Overcoming synthetic metastabilities and revealing metal-to-insulator transition & thermistor bi-functionalities for d-band correlation perovskite nickelates†

Jikun Chen,^{‡*a} Haiyang Hu,^{‡a} Jiaou Wang,^b Takeaki Yajima,^c Binghui Ge,^d
Xinyou Ke,^e Hongliang Dong,^f Yong Jiang^{*a} and Nuofu Chen^{*g}

Effective synthesis of meta-stable materials challenging the thermodynamic limits will play a significant role in broadening the horizon in material designs and further explorations of their functionalities. Although d-band correlated rare-earth nickelate perovskites (ReNiO₃) have achieved promising applications, e.g., metal-to-insulator transition, artificial intelligence, and memory/logical devices, the thermodynamic instability and high vacuum-dependence in material synthesis have largely caused bottlenecks in these applications. Herein we demonstrate a vacuum-free and low cost chemical route to effectively synthesize single-crystalline ReNiO₃ thin films that further promote their device applications. It achieves high flexibility and convenience by adjusting the A-site compositions within the perovskites *via* single (*i.e.* Nd, Sm, Eu, and Gd), binary (*i.e.*, Sm_{1-x}Nd_x and Sm_{1-x}Eu_x) and triple (*i.e.* Sm_{1-x-y}Nd_xEu_y and Sm_{1-x-y}Nd_xGd_y) rare-earth elements. The respective regulations in electronic structures, as probed *via* near edge X-ray absorption fine structure analysis, result in sharper metal-to-insulator transitions within a broad temperature range of 400 K, compared with their reported performances. Furthermore, we discover an overlooked thermistor transport behavior of ReNiO₃ within the binary A-site elements, which exhibits large temperature coefficients of resistance (> 2%) across a broad range of temperatures (5–470 K). By overcoming the bottlenecks in material synthesis of ReNiO₃, the present work profoundly paves the way for device fabrication.

Challenging thermodynamic limits and synthesizing materials at their meta-stable states can largely broaden the horizons in

Conceptual insights

We utilize the film/substrate interfacial coherency achieved *via* chemical routes to overcome the high thermodynamic metastability in thin film growth of d-band correlated perovskite nickelates. For the first time, a simple and non-vacuum chemical route was developed to effectively synthesize quasi-single crystalline thin films of a series of perovskite nickelates with single, binary and triple rare-earth compositions that can be effectively and flexibly adjusted. Considering the solid base of the sufficiently improved material synthesis for rare-earth nickelates, we achieve a metal to insulator transition sharpness that is comparable to the best ones ever reported for rare-earth nickelates, while their transition temperature is widely adjustable across a wide temperature range of 400 K. Furthermore, we discovered the high temperature sensitivity of the orbital configurations that can gradually transit even without reaching the critical temperature in typical d-band correlated conductive oxides, as overlooked previously. This enriches a new functionality of thermistor transport for the rare-earth nickelate thin films grown presently, and the as-achieved TCR across a broad temperature range is not achievable conventionally. Combining both functionalities of the thermistor transport and metal-to-insulator transitions opens a new gate in designing emerging devices for Joule energy sensing, artificial intelligence and temperature driven memory/logical devices.

designing the next-generation new materials, such as ultra-strong metals,^{1,2} multi-functional oxides,³ semiconductors with irregular orbital configurations,^{4,5} and ultralight structural materials.⁶ One of the most notable meta-stable material families is the perovskite structured rare-earth nickelates (ReNiO₃) with d-band electron correlations. It is well known that ReNiO₃

^a Beijing Advanced Innovation Center for Materials Genome Engineering, School of Materials Science and Engineering, University of Science and Technology Beijing, Beijing 100083, China. E-mail: jikunchen@ustb.edu.cn, yjiang@ustb.edu.cn

^b Beijing Synchrotron Radiation Facility, Institute of High Energy Physics, Chinese Academy of Sciences, Beijing 100049, China

^c School of Engineering, The University of Tokyo, 2-11-16 Yayoi, Bunkyo-ku, Tokyo 113-0032, Japan

^d Institute of Physical Science and Information Technology, Anhui University, 230601, Hefei, Anhui, China

^e Department of Mechanical and Aerospace Engineering, Case Western Reserve University, Cleveland, Ohio 44106, USA

^f Center for High Pressure Science and Technology Advanced Research, Shanghai 201203, China

^g School of Renewable Energy, North China Electric Power University, Beijing 102206, China. E-mail: nfchen@ncepu.edu.cn

† Electronic supplementary information (ESI) available. See DOI: 10.1039/c9mh00008a

‡ J. Chen and H. Hu contributed equally to this work.

exhibits metal-to-insulator transitions (MITs) that can be triggered by variations in temperature, and this enriches electrical, optical and magnetic functionalities beyond conventional semiconductors.^{7–15} The orbital configurations and electronic band structures of ReNiO_3 are largely determined by the bond angle of Ni–O–Ni within the NiO_6 octahedron.^{10–13} Owing to the coupling between the electronic structure and structures in ReNiO_3 , their metal to insulator transition temperature (T_{MIT}) can be effectively regulated within a broad range of temperature from 100 to 600 K continuously, by simply varying the rare-earth composition.^{11–13} This distinguished feature can be potentially applied in thermal or temperature driven devices,^{11–13} competing with vanadium oxides. In addition, ReNiO_3 also exhibits complex electronic phase diagrams that are exceptionally sensitive to other parameters, such as electrostatic polarizations,^{7,9} lattice distortions,¹¹ and orbital occupancy.⁸ Utilizing a static electronic field or hydrogenation to regulate the orbital configurations in ReNiO_3 results in other interesting applications, such as memory devices,^{7,8} solid state energy conversion devices,¹⁶ biological sensing,¹⁷ and neuron-spin logical devices.¹⁸ These recent demonstrations promote further explorations of new generation electronic and optoelectronic devices based on the electron correlated perovskite systems.^{7,8,15–19}

Nevertheless, the present ineffectiveness in the thin film growth of ReNiO_3 with a high thermodynamic instability, *i.e.*, $\text{Re} = \text{Sm}, \text{Eu}$ or Gd , remains a vital bottleneck for their further device applications. In contrast to the conventional oxide materials, the crystallization and material growth of ReNiO_3 *via* the conventional chemical reactions under usual conditions is restricted, owing to their positive formation free energy (ΔG).^{11–14} To date, the thin film growth of ReNiO_3 is heavily dependent on vacuum-based approaches, such as pulsed laser deposition (PLD),^{9,20,21} magnetic sputtering or magnetic sputtering followed by high pressure annealing^{7,8,14–18,29} and metal–organic chemical vapor deposition (MOCVD).¹⁰ Performing these vacuum depositions relies on vacuum systems, such as a vacuum chamber and pumps, and this elevates the cost and complexity in the deposition of ReNiO_3 . Therefore, the effectiveness of the thin film growth of ReNiO_3 is expected to be improved if the vacuum deposition can be replaced by a chemical solution based spin coating procedure.

Here we developed a low-cost and vacuum-free approach based on wet-chemical and high-pressure solid-state reaction processes, to effectively grow ReNiO_3 thin films with single crystallinity and extensively adjustable rare-earth compositions, including Nd , Sm , Eu , Gd , $\text{Sm}_{1-x}\text{Nd}_x$, $\text{Sm}_{1-x}\text{Eu}_x$, $\text{Sm}_{1-x-y}\text{Nd}_x\text{Eu}_y$ and $\text{Sm}_{1-x-y}\text{Nd}_x\text{Gd}_y$. Sharp and widely tunable MIT properties were achieved within a broad range of temperature from 100–500 K, by regulating the Re compositions and film/substrate interfacial strains. The respective variations in electronic structures of ReNiO_3 were further investigated assisted by near edge X-ray absorption fine structure (NEXAFS) analysis. In addition to their metal to insulator transitions, an additional functionality associated with the thermistor transportation was discovered within the insulating phase of highly metastable ReNiO_3 with a small size of the rare-earth element. The achieved temperature

coefficient of resistance (TCR) exceeds 2% across a broad temperature range (5–480 K), shedding light on applying the as-grown ReNiO_3 as a Joule sensor for the detection of temperature and thermal perturbations.

The main challenge that impedes synthesizing the perovskite structured ReNiO_3 ($\text{Re} \neq \text{La}$) *via* the conventional chemical processes is associated with their positive formation free energies (ΔG).^{11–14} The LaNiO_3 is known to be the only thermodynamically stable one within the family of ReNiO_3 , and further reducing the radius of Re enhances the positive magnitude of ΔG and elevates the metastability.¹⁴ This is demonstrated in Fig. 1a, where the relative elevation in ΔG compared to that of LaNiO_3 is calculated for ReNiO_3 and plotted as a function of the size of the rare-earth elements. In this work, the element transfer of Re and Ni to the substrate for the thin film growth of ReNiO_3 was achieved by spin coating a chemical solution that contains precursors of $\text{Re}(\text{NO}_3)_3$ and $\text{Ni}(\text{CH}_3\text{COO})_2$ dissolved in ethylene glycol monomethyl ether (EGME), as illustrated in Fig. 1b. The rare-earth compositions in the as-grown ReNiO_3 can be easily adjusted by varying the types and combinations of the $\text{Re}(\text{NO}_3)_3$ chemical precursor. The crystallization of ReNiO_3 from the chemical precursors is illustrated at the bottom of Fig. 1b. From the thermodynamic perspective, the ΔG is reduced *via* a heterogeneous nucleation of ReNiO_3 onto the lattice template of the perovskite structured substrate,^{10,13,20,21} combined with the utilization of high oxygen pressures.^{11–14} From the kinetic perspective, elevating the synthetic temperature promotes the migration of the lattice atoms during the thin film growth.

The proposed approach was first applied to the thin film growth of SmNiO_3 on single crystalline perovskite substrates, such as LaAlO_3 (LAO), SrTiO_3 (STO) and $(\text{La,Sr})(\text{Al,Ta})\text{O}_3$ (LSAT), with an orientation of (001). The lattice constants of LAO, STO and LSAT are 3.79 Å, 3.905 Å, and 3.87 Å, respectively, and these numbers are similar to the half magnitude of the phase diagonal of SmNiO_3 (3.807 Å). Therefore, a heterogeneous film growth of SmNiO_3 on these substrates is expected that reduces the formation free energy. The X-ray diffraction (XRD) patterns and reciprocal space mapping (RSM) of the as-grown SmNiO_3 on various substrates are shown in Fig. 1c and d, respectively. In XRD, the diffraction peak associated with the film mainly appears besides the ones for the substrates, indicating a similar cross-plane orientation to that of the as-grown SmNiO_3 with the three perovskite substrates (see XRD patterns at a broader scanning range in Fig. S1, ESI†). The state of interfacial strain between the as-grown SmNiO_3 and the perovskite substrates is further indicated by their RSM results as shown in Fig. 1d. For $\text{SmNiO}_3/\text{LAO}$, a similar in-plane reciprocal lattice vector (Q_{\parallel}) is observed for the film and the substrate, which indicates that the in-plane lattice of SmNiO_3 is locked by the one of LaAlO_3 and the as-grown thin film is under bi-axially compressive distortion. In contrast, the diffraction patterns associated with the films observed for $\text{SmNiO}_3/\text{STO}$ and $\text{SmNiO}_3/\text{LSAT}$ are elongated. This indicates that the interfacial strain between the film and the substrate is relaxed, in which case no effective tensile distortion is imparted upon the film material. Fig. 1e further shows the cross-section morphology of the $\text{SmNiO}_3/\text{LAO}$

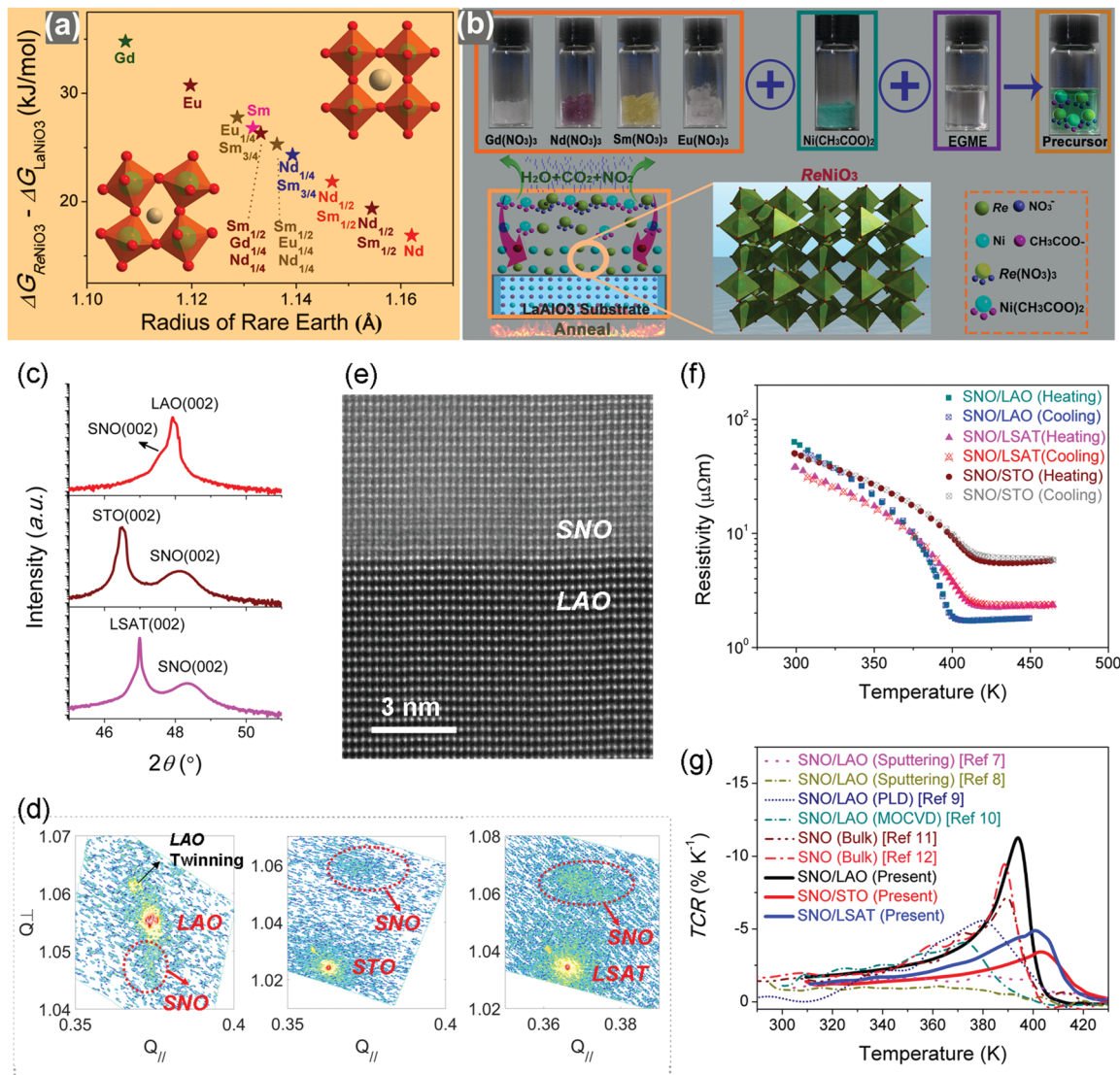


Fig. 1 (a) The relative formation free energy of ReNiO_3 as compared to LaNiO_3 ; (b) schematic illustration of the as-proposed deposition approach based on wet chemical processes. The precursors of $\text{Re}(\text{NO}_3)_3$ and $\text{Ni}(\text{CH}_3\text{COOH})_2$ were mixed together with other chemical additives and made into liquid solutions (their photos are shown in the top figure). The as made chemical solution was spin coated onto $\text{LaAlO}_3(001)$ for element transfer of the film materials, followed by annealing at 800°C under a high pressure oxygen atmosphere for crystallization (illustrated by the bottom figures); (c) the X-ray diffraction patterns and (d) reciprocal space mappings (RSM) of as-grown SmNiO_3 (SNO) on the LaAlO_3 (LAO), SrTiO_3 (STO) and $(\text{LaAlO}_3)_{0.3}(\text{Sr}_2\text{AlTaO}_6)_{0.7}$ (LSAT) substrates with a (001) orientation; (e) the high-angle annular dark-field (HAADF) images of the interfacial regions of SNO/LAO; (f) temperature dependence of the resistivity for SNO/LAO, SNO/STO and SNO/LSAT; (g) temperature coefficients of resistance (TCR) of the presently grown SNO, as compared to the previous work.^{7–12}

interface, which demonstrates a coherent growth of single crystalline SmNiO_3 on the surface of the LAO substrate. This differs from the cross-section morphology observed in $\text{SmNiO}_3/\text{STO}$ (see Fig. S2, ESI[†]), in which case the lattice coherency is largely destroyed owing to strain relaxation.

The MIT behavior of the as-grown SmNiO_3 on various substrates was characterized by measuring the resistivity as a function of temperature (R - T tendency) *via* both heating up and cooling down processes as shown in Fig. 1f. It can be seen that all samples exhibit a pronounced transition behavior in their electrical transportations across the transition temperature (T_{MIT}), while their R - T tendency measured *via* heating up and

cooling down overlaps well with each other. Compared to the strain relaxed $\text{SmNiO}_3/\text{LSAT}$ or $\text{SmNiO}_3/\text{STO}$, the compressively distorted $\text{SmNiO}_3/\text{LAO}$ exhibits a sharper MIT behavior and a lower T_{MIT} , as demonstrated by their temperature dependence of TCR in Fig. 1g. These observations are in agreement with the previous reports that the compressive distortion enhances the relative stability in the metallic phase of ReNiO_3 .^{7–15} It is worth noticing that the usage of high oxygen pressure and the lattice template effect are both important to achieve a sharp MIT behavior for the as-grown SmNiO_3 (see more discussions in the ESI[†]).

The above synthetic approach was further extended to the growth of ReNiO_3 thin films with more combinations of

rare-earth compositions, including NdNiO_3 , EuNiO_3 , GdNiO_3 , $\text{Sm}_{0.75}\text{Nd}_{0.25}\text{NiO}_3$, $\text{Sm}_{0.5}\text{Nd}_{0.5}\text{NiO}_3$, $\text{Sm}_{0.25}\text{Nd}_{0.75}\text{NiO}_3$, $\text{Sm}_{0.75}\text{Eu}_{0.25}\text{NiO}_3$, $\text{Sm}_{0.5}\text{Eu}_{0.25}\text{Nd}_{0.25}\text{NiO}_3$, and $\text{Sm}_{0.5}\text{Gd}_{0.25}\text{Nd}_{0.25}\text{NiO}_3$, on LAO (001). In this work, this was achieved by simply varying the composition and combination of the as-used $\text{Re}(\text{NO}_3)_3$ precursors within the solution, and therefore effective regulations in their T_{MIT} within a broad range of temperature were expected. Fig. S3 and S4 (ESI[†]) show the XRD patterns of the presently grown $\text{ReNiO}_3/\text{LAO}$ with single and binary rare-earth compositions,

respectively, while their representative RSM results are demonstrated in Fig. S5 (ESI[†]). It is worth noting that all the as-grown ReNiO_3 films exhibit the same in-plane diffraction vector on the LAO substrate, indicating their coherent epitaxy and quasi-single crystallinity.

As their R - T tendencies are shown in Fig. 2a, the presently grown $\text{ReNiO}_3/\text{LaAlO}_3$ samples exhibit MIT behavior with comparable transition sharpness and adjustable T_{MIT} similar to the previously reported ones observed in the vacuum-grown ReNiO_3 .^{7–13}

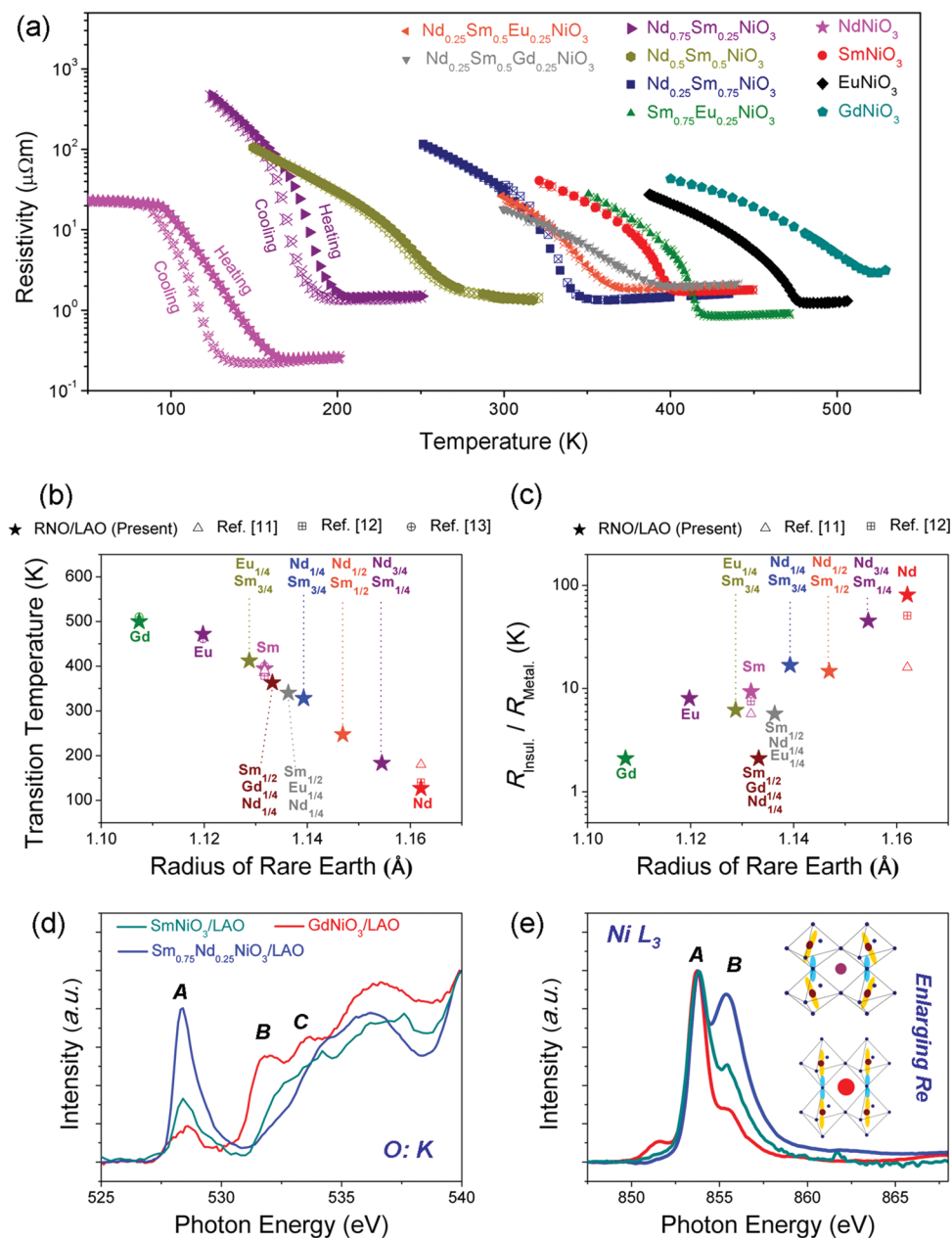


Fig. 2 (a) Temperature dependence of the resistivity for $\text{ReNiO}_3/\text{LAO}$ with various combinations of single, binary and triple elements; (b) the transition temperature (T_{MIT}) and (c) the variation in resistivity (R) across the transition ($R_{\text{insul.}}/R_{\text{metal.}}$) for the presently grown $\text{ReNiO}_3/\text{LAO}$ as compared to the previous work. The T_{MIT} was the respective temperature when the TCR reached the maximum, while the magnitudes of $R_{\text{insulating}}$ and R_{metal} were determined by elongating the R - T tendencies associated with the insulating and conductive phases, respectively, to T_{MIT} . The open symbols represent the respective magnitudes from the previous reports.^{11–13} (d and e) Near edge X-ray absorption fine structure (NEXAFS) analysis of (d) Ni- L_3 edge and (e) O-K edge of $\text{ReNiO}_3/\text{LAO}$ with various rare-earth elements.

Simply varying the relative ratio of different Re elements can achieve a continuous adjustment in T_{MIT} within a broad range of temperature from 100–500 K, which is in agreement with the previous reports on multi-element rare-earth nickelates.^{11,13,30} It is also interesting to note that a pronounced hysteresis in T_{MIT} was observed for NdNiO_3 and $\text{Nd}_{0.75}\text{Sm}_{0.25}\text{NiO}_3$ when measuring their R - T *via* heating up compared to cooling down. In contrast, the R - T measured *via* heating up or cooling down nearly overlap with each other for ReNiO_3 with smaller rare-earth elements occupying the A-site of the perovskite structure. In Fig. 2b and c, we further summarize the T_{MIT} and the variation in resistivity across the transition ($R_{\text{insul.}}/R_{\text{metal}}$), respectively. It clearly demonstrates a reducing tendency in T_{MIT} when enlarging the average radius of the rare-earth elements, which is in agreement with the previous reports.^{11,13,30} For ReNiO_3 with a single elemental rare-earth composition, a more significant variation in the resistivity during MIT was observed for the compositions with larger Re. In addition, the magnitude of $R_{\text{insul.}}/R_{\text{metal}}$ is observed to be smaller when mixing various Re within ReNiO_3 . The widely tunable metal to insulator transitions as achieved in ReNiO_3 cater to further electronic applications, such as temperature switches and suppression of the inrush current.

From the perspective of electron orbital configuration and band structure, reducing the size of Re was known to twist the NiO_6 octahedron more and bend the Ni–O–Ni bonds, which splits a wider energy gap within the hybridized O-2p and Ni-3d.^{11–14} As a result, the orbital configurations associated with the insulating states (denoted as Ni^{3+}) are strengthened, as compared to the ones for the metallic states (denoted as Ni^{2+}),^{8,13} leading to an elevation in T_{MIT} when reducing the size of Re. Near edge X-ray absorption fine structure (NEXAF) analysis was previously reported to be an effective approach to probe the proportion of orbital configurations between the metallic and insulating states.^{22–25} Therefore, NEXAF was further performed to investigate the O: K-edge and Ni: L-edge of ReNiO_3 with various compositions of Re, and the results are shown in Fig. 2d and e, respectively. Following the previous argument, a larger proportion of the metallic orbital configurations compared to the insulating one is expected for ReNiO_3 with a larger size of the rare-earth elements that more straightened the Ni–O–Ni bonds.^{11–14} Comparing the O: K-edge EXAFS spectra of GdNiO_3 and SmNiO_3 to that of $\text{Sm}_{3/4}\text{Nd}_{1/4}\text{NiO}_3$ (with an increased rare-earth size) in Fig. 2d, we can clearly see an increased pre-peak (marked as A) in the spectrum for ReNiO_3 with a larger Re. In their O: K-edge spectrum, the pre-peak A is largely related to the Ni^{3+} (d^8L) configuration, while peaks B and C are associated with the Ni^{2+} (d^9L) configuration.^{22,25} The enhanced proportion in the ground state of Ni^{3+} as compared to Ni^{2+} indicates a more strengthened metallic phase as compared to the insulating phase, which is in agreement with the reduction in their T_{MIT} as shown in Fig. 2a. Further consistency was observed from variations in their Ni: L_3 spectrum, which originates from the Ni-2p \rightarrow Ni-3d transition and splits into peaks A and B (see Fig. 2e). The proportion of the $t_{2g}^2e_g^1$ (Ni^{3+}) orbital configurations compared to the $t_{2g}^2e_g^2$ (Ni^{2+}) one is known

to be indicated from the relative height of peak B split from peak A in the Ni: L_3 NEXAFS spectrum.^{22–24} Comparing the Ni: L_3 -edge NEXAFS spectrum as shown in Fig. 2e, an increasing tendency in peak B is clearly observed when increasing the average radius of Re.

The enhanced effectiveness in growing meta-stable ReNiO_3 thin films of single crystallinity further paves the way for exploring their practical applications in emerging electronic devices. Apart from their abrupt orbital transitions near T_{MIT} as known previously, we highlight the temperature sensitivities in electrical transportations observed in the insulating phase of ReNiO_3 owing to gradual orbital transitions covering a broader range of temperatures. In the conventional semiconductors, elevating the temperature results in a thermally intrinsic (or extrinsic) activation of carriers from the valence band (or dopant band) to the conduction band, as illustrated in Fig. 3a. The resultant R - T tendency follows $R \propto T^{-3/2} \exp\left(\frac{E_g}{k_B T}\right)$, and the as-achieved magnitude of TCR does not exceed $-2\% \text{ K}^{-1}$, as estimated in Fig. S6 (ESI[†]) for various magnitudes of the band gap (E_g).

In contrast to the conventional semiconductors, the transportation properties associated with the orbital configuration and the band structure of ReNiO_3 are closely coupled to the structure of the NiO_6 octahedron and the Ni–O bond angles.^{11–13} The most typical example is the MIT behavior observed when reducing the temperature across T_{MIT} , in which case an abrupt straightening of the bond angle of Ni–O–Ni occurs that opens a band gap to trigger an electronic transition from the metallic phase to the insulating phase.¹³ This was also comprehended previously as a charge disproportionation of the transition metal ($2\text{Ni}^{3+} \rightarrow \text{Ni}^{3+\delta} + \text{Ni}^{3-\delta}$) accompanied by a Jahn–Teller distortion within the NiO_6 octahedron to reduce the Coulomb repulsion energy associated with the hybridized Ni-3d and O-2p orbital configurations.³¹ By elevating the temperature even without reaching T_{MIT} , the system's Coulomb energy is expected to be accumulated within the insulating phase of ReNiO_3 to result in a gradual orbital transition. This is also revealed by the temperature varied Ni–O vibration modes as previously observed in the insulating phase of SmNiO_3 *via* temperature dependent Raman spectroscopy,³² showing that the structure of the NiO_6 octahedron largely determines the orbital configuration and the band structure. Therefore, a more susceptible band structure to temperature is expected for the insulating phase of ReNiO_3 compared to the conventional semiconductors (as illustrated in the right of Fig. 3a), which enlarges the R - T tendency and the magnitude of TCR.

The above understandings are supported by the low temperature R - T tendencies observed in the representative ReNiO_3 with single or binary rare-earth compositions. As shown in Fig. 3b, a continuous reducing tendency in the resistivity is observed for the insulating phases of SmNiO_3 , EuNiO_3 and $\text{Nd}_x\text{Sm}_{1-x}\text{NiO}_3$ across a broad range of low, mid-low and room temperatures. In Fig. S7 (ESI[†]), the presently observed R - T tendencies were fitted by $R(T)/R_{\text{metal}} = \exp\left(\frac{E_a}{k_B T}\right)$, which describes the transportations for conventional thermistors with a negative temperature coefficient of resistance (NTCR).

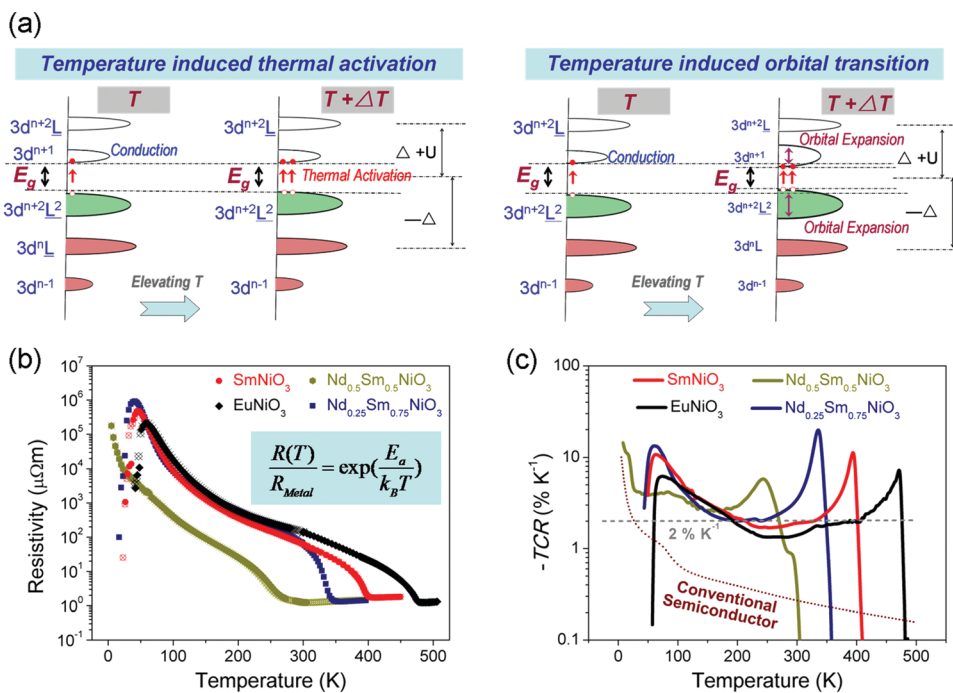


Fig. 3 (a) Illustrating the migration of electrons from the valence band to the conduction band associated with the thermal activation (left) and orbital transitions (right) when elevating the temperature. (b) Temperature dependence of resistivity and (c) temperature coefficient of resistance of ReNiO_3 with various combinations of the rare-earth elements, compared to conventional semiconductors via thermal activation of the carriers.

In contrast to the conventional semiconductors, the activation energy (E_a) calculated for the present ReNiO_3 samples is temperature dependent (see Fig. S7c, ESI[†]), implying their temperature varied orbital configurations and band gaps. Compared to SmNiO_3 or NdNiO_3 with a single Re composition, the $\text{Nd}_{0.25}\text{Sm}_{0.75}\text{NiO}_3$ with a binary Re composition exhibits a larger magnitude of TCR exceeding 2% across a broad range of temperatures from 40 to 340 K, as shown in Fig. 3c. This performance is comparable to the best negative temperature coefficient thermistor at a similar wide range of working temperatures.^{26,27} Near room temperature, the as achieved TCR in $\text{Nd}_{0.25}\text{Sm}_{0.75}\text{NiO}_3$ further increases up to $\sim 4\%$, and this performance is comparable to that of VO_2 which is presently applied in the non-cooling detection of infrared rays (IR).^{27,28}

The large TCR within a broad range of temperatures achieved in the insulating phase of the ReNiO_3 materials indicates their thermistor functionality that can be used to sense the temperature or incident thermal perturbations via their resultant variations in resistivity. This further sheds light on their thermistor applications such as temperature detection and sensing, temperature compensation, and infrared ray detection.^{26–28} Fig. S8 (ESI[†]) illustrates one such example associated with the detection of temperature and thermal perturbations via ReNiO_3 . Similar to their MIT, the range of working temperatures when using the insulating phase of ReNiO_3 as a thermistor is widely adjustable via the rare-earth compositions to cater for the practical requirements. For example, enhancing the Nd substitution concentration within $\text{Nd}_x\text{Sm}_{1-x}\text{NiO}_3$ can effectively extend the lower limit of the applicable range down to 5 K, while the upper limit of the applicable temperature range can be extended up to 470 K via using EuNiO_3 .

In summary, we developed a vacuum-free approach combining spin coating and high oxygen pressure solid state reactions to efficiently grow quasi-single crystalline ReNiO_3 (Re = Nd, Sm, Eu, Gd, $\text{Sm}_{1-x}\text{Nd}_x$ and $\text{Sm}_{1-x}\text{Eu}_x$, $\text{Sm}_{1-x-y}\text{Nd}_x\text{Eu}_y$ and $\text{Sm}_{1-x-y}\text{Nd}_x\text{Gd}_y$) thin films, overcoming their high thermodynamic metastability. The metal to insulator transition performance achieved in the as-grown ReNiO_3 is comparable to the ones reported for the vacuum deposited samples. By simple regulation of the composition and combinations of rare-earth elements, effective regulation of T_{MIT} was achieved within a broad range of temperatures from 100–500 K. Results from NEXAFS further demonstrated the consistency in the variation of orbital configurations associated with the metallic and insulating states when varying the rare-earth compositions. In addition to the already known MIT behavior of ReNiO_3 driven by the abrupt orbital transitions across T_{MIT} , we also highlight the presence of a gradual orbital transition within their insulating phase over a much broader range of temperatures. This results in a thermistor transportation behavior with a large magnitude and a widely tunable temperature coefficient of the resistance, the performance of which is comparable to the best thermistors at a similar range of working temperatures. By overcoming the bottlenecks in material synthesis, it profoundly paves the way for further applying both the metal to insulator transition and thermistor functionalities of ReNiO_3 in electronic devices.

Author contributions

JC planned for the present work and analysed the data; HH grew the thin films and characterized their transportation

property; JC and XK performed structural analysis; HD and BG contributed to the TEM experiment; JW contributed to the EXAFS experiment; and JC wrote the manuscript, assisted by NC, YJ and YT. All authors discussed the results and commented on the manuscript.

Conflicts of interest

We declare no competing financial interest.

Acknowledgements

This work was supported by the National Natural Science Foundation of China (No. 51602022 and 61674013). We appreciate helpful discussions and technical support from Prof. Jian Shi (RPI, USA) and Prof. Akira Toriumi (The University of Tokyo, Japan).

References

- 1 K. Kim, M. W. Schulze, A. Arora, R. M. Lewis III, M. A. Hillmyer, K. D. Dorfman and F. S. Bates, Thermal processing of diblock copolymer melts mimics metallurgy, *Science*, 2017, **356**, 520–523.
- 2 Z. Li, K. G. Pradeep, Y. Deng, D. Raabe and C. C. Tasan, Metastable high-entropy dual-phase alloys overcome the strength-ductility trade-off, *Nature*, 2016, **534**, 227.
- 3 J. H. Lee, G. Luo, I. C. Tung, S. H. Chang, Z. Luo, M. Malshe, M. Gadre, A. Bhattacharya, S. M. Nakhmanson, J. A. Eastman, H. Hong, J. Jellinek, D. Morgan, D. D. Fong and J. W. Freeland, Dynamic layer rearrangement during growth of layered oxide films by molecular beam epitaxy, *Nat. Mater.*, 2014, **13**, 879.
- 4 Z. Zhao, H. Zhang, D. Y. Kim, W. Hu, E. S. Bullock and T. A. Strobel, Properties of the exotic metastable ST12 germanium allotrope, *Nat. Commun.*, 2017, **8**, 13909.
- 5 C. Chen, J. Avila¹, H. Arezki, V. L. Nguyen, J. Shen, M. Mucha-Kruczyński, F. Yao, M. Boutchich, Y. Chen, Y. H. Lee and M. C. Asensio, Large local lattice expansion in graphene adlayers grown on copper, *Nat. Mater.*, 2018, **17**, 450.
- 6 M. Hu, J. He, Z. Zhao, T. A. Strobel, W. Hu, D. Yu, H. Sun, L. Liu, Z. Li, M. Ma, Y. Kono, J. Shu, H. K. Mao, Y. Fei, G. Shen, Y. Wang, S. J. Juhl, J. Y. Huang, Z. Liu, B. Xu and Y. Tian, Compressed glassy carbon: An ultrastrong and elastic interpenetrating graphene network, *Sci. Adv.*, 2017, **3**, e1603213.
- 7 J. Shi, S. D. Ha, Y. Zhou, F. Schoofs and S. Ramanathan, A correlated nickelate synaptic transistor, *Nat. Commun.*, 2013, **4**, 2676.
- 8 J. Shi, Y. Zhou and S. Ramanathan, Colossal resistance switching and band gap modulation in a perovskite nickelate by electron doping, *Nat. Commun.*, 2014, **5**, 4860.
- 9 N. Shukla, T. Joshi, S. Dasgupta, P. Borisov, D. Lederman and S. Datta, Electrically induced insulator to metal transition in epitaxial SmNiO₃ thin films, *Appl. Phys. Lett.*, 2014, **105**, 012108.
- 10 F. Conchon, A. Boule and R. Guinebretière, Effect of tensile and compressive strains on the transport properties of SmNiO₃ layers epitaxially grown on (001) SrTiO₃ and LaAlO₃ substrates, *Appl. Phys. Lett.*, 2007, **91**, 192110.
- 11 M. T. Escote, A. M. L. da Silva, J. R. Matos and R. F. Jardim, General properties of polycrystalline LnNiO₃ (Ln = Pr, Nd, Sm) compounds prepared through different precursors, *J. Solid State Chem.*, 2000, **151**, 298–307.
- 12 I. V. Nikulina, M. A. Novojilova, A. R. Kaulb, S. N. Mudretsovab and S. V. Kondrashovb, Oxygen nonstoichiometry of NdNiO₃ and SmNiO₃, *Mater. Res. Bull.*, 2004, **39**, 775–791.
- 13 G. Catalan, Progress in perovskite nickelate research, *Phase Transform.*, 2008, **81**, 729.
- 14 R. Jaramillo, F. Schoofs, S. D. Ha and S. Ramanathan, High pressure synthesis of SmNiO₃ thin films and implications for thermodynamics of the nickelates, *J. Mater. Chem. C*, 2013, **1**, 2455.
- 15 R. Jaramillo, S. D. Ha, D. M. Silevitch and S. Ramanathan, Origins of bad-metal conductivity and the insulator–metal transition in the rare-earth nickelates, *Nat. Phys.*, 2014, **10**, 304.
- 16 Y. Zhou, X. Guan, H. Zhou, K. Ramadoss, S. Adam, H. Liu, S. Lee, J. Shi, M. Tsuchiya, D. D. Fong and S. Ramanathan, Strongly correlated perovskite fuel cells, *Nature*, 2016, **534**, 231.
- 17 Z. Zhang, D. Schwanz, B. Narayanan, M. Kotiuga, J. A. Dura, M. Cherukara, H. Zhou, J. W. Freeland, J. Li, R. Sutarto, F. He, C. Wu, J. Zhu, Y. Sun, K. Ramadoss, S. S. Nonnenmann, N. Yu, R. Comin, K. M. Rabe, S. K. R. S. Sankaranarayanan and S. Ramanathan, Perovskite nickelates as electric-field sensor in salt water, *Nature*, 2018, **553**, 68.
- 18 F. Zuo, P. Panda, M. Kotiuga, J. Li, M. Kang, C. Mazzoli, H. Zhou, A. Barbour, S. Wilkins, B. Narayanan, M. Cherukara, Z. Zhang, S. K. R. S. Sankaranarayanan, R. Comin, K. M. Rabe, K. Roy and S. Ramanathan, Habituation based synaptic plasticity and organismic learning in a quantum perovskite, *Nat. Commun.*, 2017, **8**, 240.
- 19 N. Lu, P. Zhang, Q. Zhang, R. Qiao, Q. He, H. B. Li, Y. Wang, J. Guo, D. Zhang, Z. Duan, Z. Li, M. Wang, S. Yang, M. Yan, E. Arenholz, S. Zhou, W. Yang, L. Gu, C. W. Nan, J. Wu, Y. Tokura and P. Yu, Electric-field control of tri-state phase transformation with a selective dual-ion switch, *Nature*, 2017, **546**, 124.
- 20 A. Ambrosini and J. F. Hamet, Sm_xNd_{1-x}NiO₃ thin-film solid solutions with tunable metal–insulator transition synthesized by alternate-target pulsed-laser deposition, *Appl. Phys. Lett.*, 2003, **82**, 727.
- 21 F. Y. Bruno, K. Z. Rushchanskii, S. Valencia, Y. Dumont, C. Carrétéro, E. Jacquet, R. Abrudan, S. Blügel, M. Ležaić, M. Bibes and A. Barthélémy, Rationalizing strain engineering effects in rare-earth nickelates, *Phys. Rev. B: Condens. Matter Mater. Phys.*, 2013, **88**, 195108.
- 22 K. Kleiner, J. Melke, M. Merz, P. Jakes, P. Nage, S. Schuppler, V. Liebau and H. Ehrenberg, Unraveling the degradation process of LiNi_{0.8}Co_{0.15}Al_{0.05}O₂ electrodes in commercial

- lithium ion batteries by electronic structure investigations, *ACS Appl. Mater. Interfaces*, 2015, **7**, 19589.
- 23 L. A. Montoro, M. Abbate and J. M. Rosolen, Electronic structure of transition metal Ions in deintercalated and reintercalated $\text{LiCo}_{0.5}\text{Ni}_{0.5}\text{O}_2$, *J. Electrochem. Soc.*, 2000, **147**, 1651–1657.
- 24 H. Kobayashi, M. Shikano, S. Koike, H. Sakaebe and K. Tatsumi, Investigation of positive electrodes after cycle testing of high-power Li-Ion battery cells, *J. Power Sources*, 2007, **174**, 380–386.
- 25 F. Reinert, P. Steiner, S. Hüfner, H. Schmitt, J. Fink, M. Knupfer, P. Sandl and E. Bertel, Electron and hole doping in NiO, *Z. Phys. B: Condens. Matter*, 1995, **97**, 83–93.
- 26 E. Ohg, Negative temperature coefficient resistance (NTCR) ceramic thermistors: An industrial perspective, *J. Am. Ceram. Soc.*, 2009, **92**, 967–983.
- 27 A. Rogalski, Infrared detectors: an overview, *Infrared Phys. Technol.*, 2002, **43**, 187–210.
- 28 Z. Li, Z. Hu, J. Peng, C. Wu, Y. Yang, F. Feng, P. Gao, J. Yang and Y. Xie, Ultrahigh infrared photoresponse from core-shell single domain- $\text{VO}_2/\text{V}_2\text{O}_5$ heterostructure in nano-beam, *Adv. Funct. Mater.*, 2014, **24**, 1821–1830.
- 29 S. D. Ha, M. Otaki, R. Jaramillo, A. Podpirka and S. Ramanathan, Stable metal–insulator transition in epitaxial SmNiO_3 thin films, *J. Solid State Chem.*, 2012, **190**, 233–237.
- 30 R. F. Jardim, V. B. Barbeta, S. Andrade, M. T. Escote, F. Cordero and M. S. Torikachvili, Metal–insulator transition in $\text{Nd}_{1-x}\text{Eu}_x\text{NiO}_3$: Entropy change and electronic delocalization, *J. Appl. Phys.*, 2015, **117**, 17C105.
- 31 C. Girardot, J. Kreisel, S. Pignard, N. Caillault and F. Weiss, Raman scattering investigation across the magnetic and metal–insulator transition in rare earth nickelate RNiO_3 (R = Sm, Nd) thin films, *Phys. Rev. B: Condens. Matter Mater. Phys.*, 2008, **78**, 104101.
- 32 I. I. Mazin, D. I. Khomskii, R. Lengsdorf, J. A. Alonso, W. G. Marshall, R. M. Ibberson, A. Podlesnyak, M. J. Martínez-Lope and M. M. Abd-Elmeguid, Charge Ordering as Alternative to Jahn–Teller Distortion, *Phys. Rev. Lett.*, 2007, **98**, 176406.